Inorg. Chem. **2008**, *47*, 7249−7261

Energy Transfer Dynamics in Re^{I}−Based Polynuclear Assemblies: A Quantitative Application of Förster Theory

Troy E. Knight, Dong Guo, Juan Pablo Claude, and James K. McCusker*

Department of Chemistry, Michigan State University, East Lansing, Michigan 48824

Received April 16, 2008

The synthesis, structure, and photophysical properties of a new family of tetranuclear $FeRe_3$ chromophore-quencher complexes having the general form $[Fe(pyacac)_3(Re(bpy')(CO)_3)_3](OTf)_3$ (where pyacac = 3-(4-pyridyl)-acetylacetonate and bpy′ is 4,4′,5,5′-tetramethyl-2,2′-bipyridine (tmb, **1**), 2,2′-bipyridine (bpy, **2**), and 4,4′-diethylester-2,2′-bipyridine (deeb, **3**)) are reported. Time-resolved emission data acquired in room-temperature CH_2Cl_2 solutions exhibited single exponential decay kinetics with observed lifetimes of 450 ± 30 ps, 755 ± 40 ps, and 2.5 ± 0.1 ns for complexes **1**, **2**, and **3**, respectively. The emission in each case is assigned to the decay of the Re^{I}-based ^{3}MLCT excited state; the lifetimes are all significantly less than the corresponding $AlRe_3$ analogues (2250 ± 100 ns, 560 ± 30 ns, and 235 ± 20 ns for **4**, **5**, and **6**, respectively), which were also prepared and characterized. Electron transfer is found to be thermodynamically unfavorable for all three Re^{I}-containing systems: this fact coupled with the absence of optical signatures for the expected charge-separated photoproducts in the time-resolved differential absorption spectra and favorable spectral overlap between the donor emission and the acceptor absorption profiles implicates dipolar energy transfer from the Re^{I}-based excited state to the high-spin Fe^{III} core as the dominant quenching pathway in these compounds. Details obtained from the X-ray structural data of complex **2** allowed for a quantitative application of Förster energy transfer theory by systematically calculating the separation and spatial orientation of the donor and acceptor transition moment dipoles. Deviations between the calculated and observed rate constants for energy transfer were less that a factor of 3 for all three complexes. This uncommonly high degree of precision testifies to both the appropriateness of the Förster model as applied to these systems, as well as the accuracy that can be achieved in quantifying energy transfer rates if relative dipole orientations can be accounted for explicitly.

Introduction

Elucidating the mechanism of excited-state reactivity is a necessary first step for understanding and ultimately manipulating complex photoinduced chemical processes.[1–4] Accordingly, numerous fundamental studies of excited-state dynamics have been reported in the literature. Assemblies based on d^6 polypyridyl complexes of Re^{I}, Ru^{II}, and Os^{II} have garnered particular attention because of the relative stability of their excited states, well documented ground and excited-state electronic properties, and the ability one has to tune these properties through synthetic means. Both electron and energy transfer processes have been the subject of intense scrutiny. As a result, much has been learned about the factors that govern both of these types of excited-state reactions in transition-metal based systems.[5–14]

* To whom correspondence should be addressed. E-mail: jkm@chemistry.msu.edu.

(1) Alstrum-Acevedo, J. H.; Brennaman, M. K.; Meyer, T. J. *Inorg. Chem.* **2005**, *44*, 6802.
(2) Balzani, V.; Scandola, F. *Supramolecular Photochemistry*; Horwood: Chichester, U. K., 1991.
(3) Ziessel, R.; Hissler, M.; El-ghayoury, A.; Harriman, A. *Coord. Chem. Rev.* **1998**, *178*, 1251.
(4) Keefe, M. H.; Benkstein, K. D.; Hupp, J. T. *Coord. Chem. Rev.* **2000**, *205*, 201.
(5) Balzani, V.; Ceroni, P.; Juris, A.; Venturi, M.; Campagna, S.; Puntoriero, F.; Serroni, S. *Coord. Chem. Rev.* **2001**, *219*, 545.
(6) Balzani, V.; Juris, A.; Venturi, M.; Campagna, S.; Serroni, S. *Chem. Rev.* **1996**, *96*, 759.
(7) Argazzi, R.; Bertolasi, E.; Chiorboli, C.; Bignozzi, C. A.; Itokazu, M. K.; Murakami Iha, N. Y. *Inorg. Chem.* **2001**, *40*, 6885.
(8) Meyer, T. J. *Acc. Chem. Res.* **1989**, *22*, 163.
(9) De Silva, A. P.; Gunaratne, H. Q. N.; Gunnlaugsson, T.; Huxley, A. J. M.; McCoy, C. P.; Rademacher, J. T.; Rice, T. E. *Chem. Rev.* **1997**, *97*, 1515.
(10) De Cola, L.; Belser, P. *Coord. Chem. Rev.* **1998**, *177*, 301.

10.1021/ic800670b CCC: $40.75
Published on Web 07/23/2008

With regard to energy transfer, the two most important mechanisms are electron superexchange (Dexter)[15] and dipole−dipole coupling (Förster).[16] Dexter energy transfer is subject to a distance dependence that falls off as $\exp(-2r)$ due to its reliance on orbital overlap. As such, it is usually relegated to covalently linked systems in which the donor and acceptor are in close proximity (e.g., 5−10 Å or less).[17–22] Förster transfer is a through-space mechanism that occurs when the donor emission dipole nonradiatively couples to an absorptive dipole in the acceptor.[23–25] The dipolar nature of this interaction gives rise to a shallower r^{-6} dependence, allowing this mechanism to be operative over much longer distances. Förster-type reactivity is therefore usually dominant in systems that place the lowest energy excited state on an electronically isolated portion of the donor or between pairs of reactants that are separated over long distances.[26–29]

Förster theory has a direct connection to parameters that can be accessed experimentally. The energy transfer rate constant (k_{E_nT}) is described by eq 1,[30]

$$k_{E_nT} = \frac{9000 \ln(10)\kappa^2 \Phi_D J}{128\pi^5 \eta^4 N_A \tau_D R^6} \quad (1)$$

where κ^2 is the dipole orientation factor, Φ_D is the radiative quantum yield of the donor, η is the refractive index of the solvent, N_A is Avogadro's number, τ_D is the excited-state lifetime of the donor, R is the donor−acceptor separation, and J is a spectral overlap integral that essentially quantifies the resonance condition necessary for dipole−dipole coupling. This latter term can be evaluated from the spectroscopic properties of the system according to eq 2,

$$J = \int_0^\infty \frac{\bar{F}_D(\bar{\nu})\bar{\varepsilon}_A(\bar{\nu})}{\bar{\nu}^4} d\bar{\nu} \quad (2)$$

where $\bar{F}_D$ is the (normalized) emission spectrum of the donor and $\bar{\varepsilon}_A$ is the absorption profile of the acceptor in units of molar absorptivity. The orientation factor κ^2 defines the spatial relationship between the transition dipoles of the donor and acceptor. This is expressed mathematically in eq 3,

$$\kappa^2 = (\cos \Theta_T - 3 \cos \Theta_D \cos \Theta_A)^2 \quad (3)$$

where Θ_T is the angle between the transition dipole moments of the donor and the acceptor, and Θ_D and Θ_A are the angles these two transition dipoles make with a vector corresponding to their through-space connection.

Although eqs 1–3 constitute a complete description of the rate of dipolar energy transfer, quantifying the donor−acceptor distance (R) and the orientation factor (κ^2) can be quite difficult, particularly in polynuclear donor−acceptor assemblies.[31–40] Taking R as the metal−metal distance is a reasonable assumption when structural data are not available, but in the point-dipole approximation of Förster theory this may or may not accurately reflect the relevant distance in systems comprised of donor and acceptor states that are charge-transfer in nature. In addition, the orientation factor of $\kappa^2 = {}^2/_3$ typically invoked represents an isotropic value for species sampling all possible angular distributions.[41] While appropriate for bimolecular energy transfer processes, this approximation may not be reasonable given the rotational barriers that likely exist in covalently attached donor−acceptor complexes. The ambiguities that can arise with regard to these two variables often lead to a large variance between experiment and theory.

Recently, Moore et al. applied Förster theory in conjunction with molecular modeling calculations to study the energy transfer dynamics of naphthalene- and anthracene-appended Zn^{II} macrocycles.[42,43] These authors obtained excellent agreement between experiment and theory when employing quantitatively determined donor−acceptor distances and

(11) Barigelletti, F.; Flamigni, L. *Chem. Soc. Rev.* **2000**, *29*, 1.
(12) Hammarström, L. *Curr. Opin. Chem. Biol.* **2003**, *7*, 666.
(13) Reece, S. Y.; Nocera, D. G. *J. Am. Chem. Soc.* **2005**, *127*, 9448.
(14) Xu, Y. H.; Eilers, G.; Borgström, M.; Pan, J. X.; Abrahamsson, M.; Magnuson, A.; Lomoth, R.; Bergquist, J.; Polívka, T.; Sun, L. C.; Sundström, V.; Styring, S.; Hammarström, L; Åkermark, B. *Chem. Eur. J.* **2005**, *11*, 7305.
(15) Dexter, D. L. *J. Chem. Phys.* **1953**, *21*, 836.
(16) Förster, T. *Discuss. Faraday Soc.* **1959**, *27*, 7.
(17) Brown, W. R.; O'Boyle, N. M.; McGarvey, J. J.; Vos, J. G. *Chem. Soc. Rev.* **2005**, *34*, 641.
(18) Barigelletti, F.; Flamigni, L.; Balzani, V.; Collin, J.-P.; Sauvage, J.-P.; Sour, A.; Constable, E. C.; Cargill Thompson, A. M. W. *J. Am. Chem. Soc.* **1994**, *116*, 7692.
(19) Goeb, S.; De Nicola, A.; Ziessel, R.; Sabatini, C.; Barbieri, A.; Barigelletti, F. *Inorg. Chem.* **2006**, *45*, 1173.
(20) Chiorboli, C.; Bignozzi, C. A.; Scandola, F.; Ishow, E.; Gourdon, A.; Launay, J.-P. *Inorg. Chem.* **1999**, *38*, 2402.
(21) Indelli, M. T.; Scandola, F.; Collin, J.-P.; Sauvage, J.-P.; Sour, A. *Inorg. Chem.* **1996**, *35*, 303.
(22) Bilakhiya, A. K.; Tyagi, B.; Paul, P.; Natarajan, P. *Inorg. Chem.* **2002**, *41*, 3830.
(23) Scholes, G. D. *Annu. Rev. Phys. Chem.* **2003**, *54*, 57.
(24) Wong, K. F.; Bagchi, B.; Rossky, P. J. *J. Phys. Chem. A.* **2003**, *108*, 5752.
(25) Speiser, S. *Chem. Rev.* **1996**, *96*, 1953.
(26) Constable, E. C.; Handel, R. W.; Housecroft, C. E.; Morales, A. F.; Flamigni, L.; Barigelletti, F. *Dalton Trans.* **2003**, 1220.
(27) Ward, M. D.; Barigelletti, F. *Coord. Chem. Rev.* **2001**, *216*, 127.
(28) Benniston, A. C.; Harriman, A.; Li, P.; Sams, C. A. *J. Am. Chem. Soc.* **2005**, *127*, 2553.
(29) Fleming, C. N.; Dupray, L. M.; Papanikolas, J. M.; Meyer, T. J. *J. Phys. Chem. A.* **2002**, *106*, 2328.
(30) Van Der Meer, B. W.; Coker, G. I.; Chen, S.-Y. *Resonance Energy Transfer, Theory and Data*; VCH Publishers: New York, 1994.
(31) Weldon, F.; Hammarström, L.; Mukhtar, E.; Hage, R.; Gunneweg, E.; Hassnoot, J. G.; Reedijk, J.; Browne, W. R.; Guckian, A. L.; Vos, J. G. *Inorg. Chem.* **2004**, *43*, 4471.
(32) Hurley, D. J.; Tor, Y. *J. Am. Chem. Soc.* **2002**, *124*, 13231.
(33) Schmehl, R. H.; Auerbach, R. A.; Wacholtz, W. F. *J. Phys. Chem.* **1988**, *92*, 6202.
(34) Gholamkhass, B.; Nozaki, K.; Ohno, T. *J. Phys. Chem. B* **1997**, *101*, 9010.
(35) Venturi, M.; Marchioni, F.; Ferrer Ribera, B.; Balzani, V.; Opris, D. M.; Schluter, A. D. *ChemPhysChem* **2006**, *7*, 229.
(36) Furue, M.; Ishibashi, M.; Satoh, A.; Oguni, T.; Maruyama, K.; Sumi, K.; Kamachi, M. *Coord. Chem. Rev.* **2000**, *208*, 103.
(37) Furue, M.; Maruyama, K.; Kanematsu, Y.; Kushida, T.; Kamachi, M. *Coord. Chem. Rev.* **1994**, *132*, 201.
(38) Furue, M.; Naiki, M.; Kanematsu, Y.; Kushida, T.; Kamachi, M. *Coord. Chem. Rev.* **1991**, *111*, 221.
(39) Furue, M.; Yoshidzumi, T.; Kinoshita, S.; Kushida, T.; Nozakura, S.; Kamachi, M. *Bull. Chem. Soc. Jpn.* **1991**, *64*, 1632.
(40) Grosshenny, V.; Harriman, A.; Hissler, M.; Ziessel, R. *J. Chem. Soc., Faraday Trans.* **1996**, *92*, 2223.
(41) *Fluorescence Imaging Spectroscopy and Microscopy*; Wang, X. F., Herman, B., Eds.; John Wiley: New York, 1996.
(42) Moore, E. G.; Bernhardt, P. V.; Riley, M. J.; Smith, T. A. *Inorg. Chem.* **2006**, *45*, 51.
(43) Moore, E. G.; Bernhardt, P. V.; Pigliucci, A.; Riley, M. J.; Vauthey, E. *J. Phys. Chem. A.* **2003**, *107*, 8396.

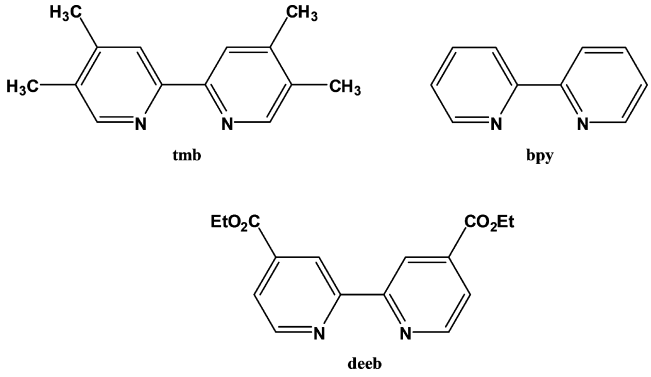

orientation factors for the various conformers identified through the modeling studies. We sought to take a similar approach in the context of an inorganic charge-transfer system. Herein, we report the synthesis, structure, and photophysical properties of a series of mixed-metal donor−acceptor assemblies: $[Fe(pyacac)_3(Re(tmb)(CO)_3)_3](OTf)_3$ (**1**), $[Fe(pyacac)_3(Re(bpy)(CO)_3)_3](OTf)_3$ (**2**), and $[Fe(pyacac)_3(Re(deeb)(CO)_3)_3](OTf)_3$ (**3**) (where pyacac = 3-(4-pyridyl)-acetylacetonate, tmb = 4,4′,5,5′-tetramethyl-2,2′-bipyridine, bpy = 2,2′-bipyridine, and deeb = 4,4′-diethylester-2,2′-bipyridine). These compounds provide a series of geometrically well-defined systems in which the donor and acceptor transition dipoles, and hence the orientation factor κ^2, can be explicitly determined. Moreover, variations in the emission energy afforded by the different bipyridyl ligands attached to the Re^I metal center provides for systematic modulation of the donor−acceptor spectral overlap. Our results demonstrate the level of agreement one can achieve between experiment and theory for this class of compounds when all of the variables involved in eq 1 are explicitly taken into account.

Experimental Section

General Information. All solvents used were purified and dried according to previously reported methods.[44] Spectroscopic grade CH_2Cl_2 was used for all photophysical measurements; the solvent was dried under CaH_2 reflux until no water was detected by ^1H NMR and degassed using freeze−pump−thaw techniques. 3-(4-pyridyl)-2,4-pentanedione,[45] $Al(pyacac)_3$,[45] $Re(tmb)(CO)_3(OTf)$,[46] $Re(bpy)(CO)_3(OTf)$,[46] $Re(deeb)(CO)_3(OTf)$,[46] and *fac*-$[Re(bpy)(CO)_3(4\text{-Etpy})](PF_6)$[47] (4-Etpy = 4-ethylpyridine) were prepared following literature procedures. 3-phenyl-2,4-pentanedione was purchased from TCI America. Elemental analyses and FT-IR data were obtained through the analytical facilities at Michigan State University. Mass spectra were obtained through the analytical facilities at The University of South Carolina.

Tris(3-(4-pyridyl)acetylacetonato)iron(III), Fe(pyacac)$_3$. The synthesis of this compound has been reported previously by a different method.[48] Amounts of 70.1 mg (0.432 mmol) of $FeCl_3$ and 230 mg (1.30 mmol) of pyacac were dissolved in 30 mL of tetrahydrofuran (THF) and stirred for 6 h, after which 125 mg (1.30 mmol) of sodium *tert*-butoxide was added to the reaction flask. The solution was then stirred overnight, filtered over celite to remove excess salt, and the solvent removed under vacuum. The product was recrystallized from CH_2Cl_2/hexanes (1:1 v/v). Yield: 131 mg (52%). Anal. Calcd for $C_{30}H_{30}N_3O_6Fe$: C, 61.65; H, 5.17; N, 7.19. Found: C, 61.49; H, 5.13; N, 7.07.

Tris(3-phenyl-acetylacetonato)iron(III), Fe(phacac)$_3$. This compound was prepared analogous to $Fe(pyacac)_3$.[48] Yield: 238 mg (78%). Anal. Calcd for $C_{33}H_{33}O_6Fe$: C, 68.16; H, 5.72. Found: C, 68.11; H, 5.79.

$[Fe(pyacac)_3(Re(tmb)(CO)_3)_3](OTf)_3$ (1). An amount of 230 mg (0.360 mmol) of $Re(tmb)(CO)_3(OTf)$ was dissolved in 75 mL of hot THF, after which 70 mg (0.12 mmol) of $Fe(pyacac)_3$ was added and the solution purged with argon for 20 min. The reaction mixture was fit with a condenser and stirred under argon for 3 days in hot THF in the dark, during which time a red solution formed along with an orange precipitate. The precipitate was collected and the filtrate was concentrated under vacuum to yield additional orange solid. The combined precipitates were dissolved in CH_2Cl_2, filtered through celite, and the solvent removed under vacuum. The product was recrystallized several times from CH_2Cl_2/pentane (1:1 v/v). Yield: 155 mg (52%). Anal. Calcd for $C_{84}H_{78}N_9F_9O_{24}S_3FeRe_3$: C, 40.70; H, 3.17; N, 5.08. Found: C, 40.36; H, 3.23; N, 4.86. IR (KBr, cm^{-1}): 2031 s, 1918 s, 1614 m, 1566 s, 1448 m, 1365 m, 1263 s, 1155 m, 1032 s, 638 m. MS: [ESI, *m*/*z* (rel. int.)]: 677.3 (70) $\{[Fe(pyacac)_3(Re(tmb)(CO)_3)_3]\}^{3+}$, 1090.5 (23) $\{[Fe(pyacac)_3(Re(tmb)(CO)_3)_3(OTf)\}^{2+}$, 2330.1 (1) $\{[Fe(pyacac)_3(Re(tmb)(CO)_3)_3](OTf)_2\}^{+}$.

$[Fe(pyacac)_3(Re(bpy)(CO)_3)_3](OTf)_3$ (2). In 25 mL of THF were dissolved 70 mg (0.12 mmol) of $Fe(pyacac)_3$ and 210 mg (0.365 mmol) of $Re(bpy)(CO)_3(OTf)$. The solution was flushed with argon for 20 min then stirred in the dark for 3 days at room temperature. An orange solid that precipitated out of solution was collected and washed with hexanes. The solid was dissolved in CH_3CN, filtered through celite, and the solvent removed under vacuum. The product was recrystallized several times from acetonitrile/ether (1:1 v/v). X-ray quality crystals were obtained by slow diffusion of ether into an acetonitrile solution of the compound. Yield: 166 mg (60%). Anal. Calcd for $C_{72}H_{54}N_9F_9O_{24}S_3FeRe_3$: C, 37.37; H, 2.35; N, 5.45. Found: C, 37.00; H, 2.23; N, 5.27. IR (KBr, cm^{-1}): 2033 s, 1922 s, 1568 m, 1446 m, 1367 w, 1261 m, 1159 m, 1032 m, 771 m, 638 m. MS: [ESI, *m*/*z* (rel. int.)]: 621 (100) $\{[Fe(pyacac)_3(Re(bpy)(CO)_3)_3]\}^{3+}$, 1006 (18) $\{[Fe(pyacac)_3(Re(bpy)(CO)_3)_3](OTf)\}^{2+}$, 2161.1 (1) $\{[Fe(pyacac)_3(Re(bpy)(CO)_3)_3](OTf)_2\}^{+}$.

$[Fe(pyacac)_3(Re(deeb)(CO)_3)_3](OTf)_3$ (3). Amounts of 29 mg (0.050 mmol) of $Fe(pyacac)_3$ and 108 mg (0.150 mmol) of $Re(deeb)(CO)_3(OTf)$ were dissolved in 25 mL of THF. The solution was flushed with argon for 20 min and the reaction mixture stirred in the dark for 4 days at room temperature. The solution was then filtered over celite and the solvent removed under vacuum to give a red solid. The product was recrystallized several times using CH_2Cl_2/pentane (1:1 v/v). Yield: 65 mg (48%). Anal. Calcd for $C_{90}H_{78}N_9F_9O_{36}S_3FeRe_3 \cdot 3CH_2Cl_2$: C, 38.00; H, 2.79; N, 4.15. Found: C, 38.00; H, 2.93; N, 4.32. IR (KBr, cm^{-1}): 2036 s, 1923 s, 1732 s, 1566 s, 1462 m, 1263 s, 1153 m, 1032 s, 767 m, 638 m. MS: [ESI, *m*/*z* (rel. int.)]: 765.4 (75) $\{[Fe(pyacac)_3(Re(deeb)(CO)_3)_3]\}^{3+}$, 1222.6 (19) $\{[Fe(pyacac)_3(Re(deeb)(CO)_3)_3](OTf)\}^{2+}$, 2594.2 (1) $\{[Fe(pyacac)_3(Re(deeb)(CO)_3)_3](OTf)_2\}^{+}$.

(44) Perrin, D. D.; Armarego, W. L. F. *Purification of Laboratory Chemicals*, 3rd ed.; Pergamon Press: Oxford, U. K., 1988.
(45) Mackay, L. G.; Anderson, H. L.; Sanders, J. K. M. *J. Chem. Soc., Perkin Trans. 1*. **1995**, *18*, 2269.
(46) Hino, J. K.; Della Ciana, L.; Dressick, W. J.; Sullivan, B. P. *Inorg. Chem.* **1992**, *31*, 1072.
(47) Caspar, J. V.; Meyer, T. J. *J. Phys. Chem.* **1983**, *87*, 952.
(48) Vreshch, V. D.; Lysenko, A. B.; Chernega, A. N.; Howard, J. A. K.; Krautscheid, H.; Sieler, J.; Domasevitch, K. V. *Dalton Trans.* **2004**, 2899.

[Al(pyacac)$_3$(Re(tmb)(CO)$_3$)$_3$](OTf)$_3$ (4). This compound was prepared analogous to compound **1** by replacing Fe(pyacac)$_3$ with Al(pyacac)$_3$. After stirring for 3 days, a precipitate that formed from the dark yellow solution was collected and the filtrate concentrated under vacuum to yield additional yellow solid. The combined precipitates were then redissolved in CH_2Cl_2, filtered through celite, and the solvent removed under vacuum. The product was recrystallized several times from CH_2Cl_2/pentane (1:1 v/v). Yield: 185 mg (64%). Anal. Calcd for $C_{84}H_{78}N_9F_9O_{24}S_3AlRe_3 \cdot CH_2Cl_2$: C, 40.55; H, 3.17; N, 4.95. Found: C, 40.37; H, 3.12; N, 4.95. IR (KBr, cm^{-1}): 2031 s, 1918 s, 1612 m, 1585 s, 1452 m, 1396 m, 1263 s, 1155 m, 1032 s, 638 m. MS: [ESI, *m*/*z* (rel. int.)]: 667.7 (65) {[Al(pyacac)$_3$-(Re(tmb)(CO)$_3$)$_3$]}$^{3+}$, 1076.1 (25) {[Al(pyacac)$_3$(Re(tmb)(CO)$_3$)$_3$]-(OTf)}$^{2+}$, 2301.3 (1) {[Al(pyacac)$_3$(Re(tmb)(CO)$_3$)$_3$](OTf)$_2$}$^{+}$.

[Al(pyacac)$_3$(Re(bpy)(CO)$_3$)$_3$](OTf)$_3$ (5). This compound was prepared analogous to compound **2** by replacing Fe(pyacac)$_3$ with Al(pyacac)$_3$. After stirring for 3 days, a yellow solid that had precipitated out of solution was collected and washed with hexanes. The solid was then dissolved in CH_3CN, filtered through celite, and the solvent removed under vacuum. The product was recrystallized several times from acetonitrile/ether (1:1 v/v). X-ray quality crystals were obtained by slow diffusion of ether into an acetonitrile solution of the compound. Yield: 187 mg (65%). Anal. Calcd for $C_{72}H_{54}N_9F_9O_{24}S_3AlRe_3$: C, 36.90; H, 2.39; N, 5.53. Found: C, 37.51; H, 2.35; N, 5.13. IR (KBr, cm^{-1}): 2033 s, 1920 s, 1585 s, 1446 s, 1398 s, 1263 s, 1159 s, 1029 s, 771 m, 638 s. MS: [ESI, *m*/*z* (rel. int.)]: 611.6 (100) {[Al(pyacac)$_3$(Re(bpy)(CO)$_3$)$_3$]}$^{3+}$, 991.9 (30) {[Al(pyacac)$_3$(Re(bpy)(CO)$_3$)$_3$](OTf)}$^{2+}$, 2132.9 (1) {[Al-(pyacac)$_3$(Re(bpy)(CO)$_3$)$_3$](OTf)$_2$}$^{+}$.

[Al(pyacac)$_3$(Re(deeb)(CO)$_3$)$_3$](OTf)$_3$ (6). This compound was prepared analogous to compound **3** by replacing Fe(pyacac)$_3$ with Al(pyacac)$_3$. After stirring for 4 days, the solution was filtered and the solvent removed under vacuum to yield an orange solid. The product was recrystallized several times from CH_2Cl_2/pentane (1:1 v/v). Yield: 60 mg (44%). Anal. Calcd for $C_{90}H_{78}N_9F_9O_{36}S_3AlRe_3$: C, 39.82; H, 2.90; N, 4.64. Found: C, 39.54; H, 2.85; N, 4.48. IR (KBr, cm^{-1}): 2036 s, 1930 s, 1734 s, 1585 s, 1448 s, 1273 s, 1151 m, 1032 s, 768 m, 638 m. MS: [ESI, *m*/*z* (rel. int.)]: 755.7 (42) {[Al(pyacac)$_3$(Re(deeb)(CO)$_3$)$_3$]}$^{3+}$, 1208.1 (10) {[Al(pyacac)$_3$-(Re(deeb)(CO)$_3$)$_3$](OTf)}$^{2+}$, 2565.3 (1) {[Al(pyacac)$_3$(Re(deeb)-(CO)$_3$)$_3$](OTf)$_2$}$^{+}$.

Physical Measurements: X-ray Structure Determinations. Single-crystal X-ray diffraction data for complexes **2** and **5** were acquired at the X-ray facility of Michigan State University. Diffraction data were collected on a Siemens SMART diffractometer with graphite-monochromatic Mo Kα radiation (λ = 0.71073Å). Data were collected at −100 °C by using an Oxford Cryosystems low temperature device. Crystallographic data are summarized in Table 1; selected bond distances and angles are listed in Table 2. Lattice parameters were obtained from least-squares analyses and data were integrated with the program SAINT.[49] The integration method employed a three-dimensional profiling algorithm and all data were corrected for Lorentz and polarization factors, as well as for crystal decay effects. The absorption correction program SADABS[50] was employed to correct the data for absorption effects. The structures were solved by direct methods and expanded using Fourier techniques. All structure calculations were performed with the SHELXTL 6.12 software package.[51]

(49) *SAINT*, ver 6.02a; Bruker AXS, Inc.: Madison, WI, 2000.
(50) Sheldrick, G. M. *SADABS*, ver 2.03; Bruker AXS, Inc.: Madison, WI, 2000.
(51) Sheldrick, G. M. , *SHELXTL*, ver 6.12; Bruker AXS, Inc.: Madison, WI, 2001.

Table 1. Crystallographic Data for [Fe(pyacac)$_3$(Re(bpy)(CO)$_3$)$_3$](OTf)$_3$ (**2**) and [Al(pyacac)$_3$(Re(bpy)(CO)$_3$)$_3$](OTf)$_3$ (**5**)

	2	**5**
formula	$C_{72}H_{54}N_9O_{24}F_9S_3FeRe_3$	$C_{72}H_{54}N_9O_{24}F_9S_3AlRe_3$
M_w	2310.87	2282.00
cryst syst	triclinic	triclinic
space group	$P\bar{1}$	$P\bar{1}$
T/K	173(2)	173(2)
a/Å	13.626(2)	13.534(2)
b/Å	17.676(3)	17.590(3)
c/Å	19.889(3)	19.809(3)
α/deg	89.494(3)	89.076(3)
β/deg	82.518(3)	81.890(3)
γ/deg	71.451(3)	71.053(3)
V/Å^3	4500.1(11)	4413.4(12)
Z	2	2
D_c/g cm^{-1}	1.717	1.717
$2\theta_{max}$	47	46
reflns measured	33672	36985
independent reflns	12741	12190
observed reflns [$I > 2\sigma(I)$]	6347	6354
μ(Mo Kα)/cm^{-1}	4.342	4.278
R_{int}	0.0918	0.0899
R1[a]	0.0675	0.0666
*w*R2[b]	0.1373	0.1564
GOF	1.007	1.044

[a] $R1 = \sum||F_o| - |F_c||/\sum|F_o|$. [b] $wR2 = [\sum w(F_o^2 - F_c^2)^2/\sum w(F_o^2)^2]^{1/2}$, $w = 1/[\sigma^2(F_o^2) + (aP)^2 + bP]$, where $P = [F_o^2 + 2F_c^2]/3$.

Table 2. Selected Bond Distances (Å) and Angles (deg) for [Fe(pyacac)$_3$-(Re(bpy)(CO)$_3$)$_3$](OTf)$_3$ (**2**) and [Al(pyacac)$_3$(Re(bpy)(CO)$_3$)$_3$](OTf)$_3$ (**5**)

2		**5**	
	Bond Distances (Å)		
Fe(1)−O(1)	1.992(6)	Al(1)−O(1)	1.877(10)
Fe(1)−O(2)	1.970(7)	Al(1)−O(2)	1.861(10)
Fe(1)−O(6)	1.997(6)	Al(1)−O(6)	1.871(11)
Fe(1)−O(7)	1.963(6)	Al(1)−O(7)	1.894(11)
Fe(1)−O(11)	1.981(7)	Al(1)−O(11)	1.883(12)
Fe(1)−O(12)	1.986(6)	Al(1)−O(12)	1.852(10)
Re(1)−N(1)	2.232(7)	Re(1)−N(1)	2.215(12)
Re(2)−N(4)	2.218(7)	Re(2)−N(4)	2.225(12)
Re(3)−N(7)	2.206(9)	Re(3)−N(7)	2.191(14)
Fe(1)···Re(1)	9.88	Al(1)···Re(1)	9.76
Fe(1)···Re(2)	9.88	Al(1)···Re(2)	9.74
Fe(1)···Re(3)	9.78	Al(1)···Re(3)	9.66
	Bond Angles (deg)		
O(1)−Fe(1)−O(2)	85.4(3)	O(1)−Al(1)−O(2)	90.0(4)
C(23)−Re(1)−N(1)	92.1(4)	C(23)−Re(1)−N(1)	93.0(6)
C(21)−Re(1)−N(1)	178.7(4)	C(21)−Re(1)−N(1)	177.9(7)
plane 1···plane 2[a]	280.1	plane 1···plane 2[a]	79.0
plane 1···plane 2[b]	82.5	plane 1···plane 2[b]	81.0
plane 1···plane 2[c]	68.8	plane 1···plane 2[c]	69.2

[a] Plane 1 is defined by atoms O(1), O(2), C(1), C(2), C(3), C(4), C(5); plane 2 is defined by atoms N(1), C(6), C(7), C(8), C(9), C(10). [b] Plane 1 is defined by atoms O(6), O(7), C(24), C(25), C(26), C(27), C(28); plane 2 is defined by atoms N(4), C(29), C(30), C(31), C(32), C(33). [c] Plane 1 is defined by atoms O(11), O(12), C(7), C(48), C(49), C(50), C(51); plane 2 is defined by atoms N(7), C(52), C(53), C(54), C(55), C(56).

Anisotropic thermal parameters were refined for all non-hydrogen atoms. Hydrogen atoms were localized in their calculation positions and refined by using the riding model. Further details concerning the structure determinations may be found in Supporting Information.

Electrochemistry. Electrochemical measurements were carried out in a N_2-filled drybox (Vacuum Atmospheres) using a BAS CV-50W electrochemical analyzer. A standard three-electrode arrangement was utilized consisting of Pt working and counter electrodes and a Ag/$AgNO_3$ reference electrode. Measurements were carried out in either CH_2Cl_2 or CH_3CN solutions containing 0.1 M NBu_4PF_6. The choice of solvent was dictated by the potential window required to observe a given redox couple; in cases where

Table 3. Electrochemical and Infrared Data for Complexes **1**−**6**

compound	electrochemical potential (V)			ν(CO) (cm^{-1})[a]	
	E_{ox} ($Re^{I/II}$)	E_{red} ($Fe^{III/II}$)	E_{red} ($bpy'^{0/-}$)	A′(1)	A″, A′(2)
$[Fe(pyacac)_3(Re(tmb)(CO)_3)_3](OTf)_3$ (**1**)	+1.47[b,c,d]	−0.91[e,f]	−1.84[b]	1918	2031
$[Fe(pyacac)_3(Re(bpy)(CO)_3)_3](OTf)_3$ (**2**)	+1.41[b]	−0.90[e]	−1.59[e]	1922	2033
$[Fe(pyacac)_3(Re(deeb)(CO)_3)_3](OTf)_3$ (**3**)	+1.60[b]	−0.93[e]	−1.20[e]	1923	2036
$[Al(pyacac)_3(Re(tmb)(CO)_3)_3](OTf)_3$ (**4**)	+1.37[b]		−1.82[b]	1918	2031
$[Al(pyacac)_3(Re(bpy)(CO)_3)_3](OTf)_3$ (**5**)	+1.42[b]		−1.57[b,g]	1920	2033
$[Al(pyacac)_3(Re(deeb)(CO)_3)_3](OTf)_3$ (**6**)	+1.54[b]		−1.19[b]	1930	2036

[a] Measured as pressed KBr pellets. [b] Measured in CH_3CN solution. [c] Potential in CH_2Cl_2 solution is +1.41 V. [d] Irreversible oxidation. The value reported corresponds to the peak of the observed anodic wave. [e] Measured in CH_2Cl_2 solution. [f] Potential in CH_3CN solution is −0.86 V. [g] Potential in CH_2Cl_2 solution is −1.57 V.

a compound could be examined in both solvents, differences in the observed potentials were found to be minor. Data were acquired using both cyclic and differential pulse voltammetry; the scan rate for the CV measurements was 100 mV/s. Values of the midpoint potentials obtained by the two techniques were comparable for the reversible Fe- and ligand-based reductions, whereas slightly larger differences were noted for the quasi-reversible Re-based oxidations. The potentials reported in Table 3 are based on the cyclic voltammetry measurements and are quoted relative to the ferrocene/ferrocenium couple which was used as an internal standard.

Electronic Absorption and Steady-State Emission Spectroscopies. Extinction coefficients for all compounds were acquired in CH_2Cl_2 solutions using a Hewlett-Packard 8452A diode array spectrophotometer. Steady-state emission spectra were acquired using a Spex Fluoromax fluorimeter and corrected for instrumental response using a NIST standard of spectral irradiance (Optronic Laboratories, Inc., OL220 M tungsten quartz lamp).[52a] Spectra were acquired on samples dissolved in thoroughly degassed CH_2Cl_2 under optically dilute conditions (o.d. ∼ 0.1) and sealed under an argon atmosphere in 1 cm path length quartz cuvettes.

Radiative quantum yields (Φ_r) were determined relative to *fac*-$[Re(bpy)(CO)_3(4\text{-}Etpy)](PF_6)$ ($\Phi_r = 0.18$ in CH_2Cl_2).[47] Quantum yields were calculated according to eq 4,

$$\Phi_{unk} = \Phi_{std}\frac{(I_{unk}/A_{unk})}{(I_{std}/A_{std})}\left(\frac{\eta_{unk}}{\eta_{std}}\right)^2 \quad (4)$$

where Φ_{unk} and Φ_{std} are the radiative quantum yields of the sample and the standard, respectively, I_{unk} and I_{std} represent the areas of the corrected emission profiles for the sample and the standard, A_{unk} and A_{std} are the absorbance values of the sample and the standard at the excitation wavelength, and η_{unk} and η_{std} correspond to the indices of refraction of the sample and standard solutions (taken to be equal to the neat solvents). Excitation wavelengths were 355 nm for the bpy and tmb analogues and 400 nm for the deeb analogues. The corrected excitation spectrum of *fac*-$[Re(bpy)(CO)_3(4\text{-}Etpy)](PF_6)$ in CH_2Cl_2 overlaid well with the compound's absorption spectrum over the range of wavelengths examined (355−400 nm), implying that the radiative quantum yield for *fac*-$[Re(bpy)(CO)_3(4\text{-}Etpy)](PF_6)$ does not vary significantly over this spectral window. The reported value of $\Phi_r = 0.18$ was therefore used for determining the radiative quantum yields at both λ_{ex} = 355 and 400 nm.

Radiative quantum yields are not being reported for complexes **1**−**3** because of the presence of an emissive impurity. The source of the impurity was traced to a small amount of dissociated complex present in solution, most likely generated by water in the CH_2Cl_2 solvent. Despite our best efforts at drying the CH_2Cl_2, there was an unacceptably large variance in repeated measurements of Φ_r. Because of the difference in time scales associated with excited-state decay between those emissive fragments and the intact assembly, the presence of these impurities does not significantly affect the kinetic analyses of these systems.

Values for the zero-point energy gap (E_{00}) of the Re^I-based ^{3}MLCT excited states were determined by fitting the emission profiles of complexes **4**−**6** based on the approach described by Claude and Meyer.[53] Wavelength data were converted to energy units following the correction of Parker and Rees;[54] the best fit was determined by visual inspection of the results of a least-squares minimization routine.

Time-Resolved Emission Spectroscopy. Nanosecond time-resolved emission data for the $AlRe_3$ model complexes **4**−**6** were collected using a Nd:YAG-based laser spectrometer that has been described previously.[52a] Data were acquired at room temperature in thoroughly degassed CH_2Cl_2 solutions having absorbances of ∼0.1 at the excitation wavelength (λ_{ex} = 355 nm for complexes **4** and **5** and 420 nm for complex **6**). Samples were sealed under an argon atmosphere in 1 cm path length quartz cuvettes. The decay traces correspond to an average of 250 shots of the signal probed at the emission maximum of each compound.

Picosecond time-resolved emission data for the $FeRe_3$ complexes **1**−**3** were collected using a time-correlated single photon counting (TCSPC) apparatus that has been described previously.[55] Data were acquired in thoroughly degassed CH_2Cl_2 solutions having absorbances of ∼0.1 at the excitation wavelength (λ_{ex} = 370 nm for complexes **1** and **2** and 430 nm for complex **3**). Samples were sealed under an argon atmosphere in 1 cm path length quartz cuvettes. Each reported decay trace corresponds to a signal average of six data sets, with each data set resulting from about 1 h of data acquisition time. The decay traces for all three complexes manifest a small baseline offset within the data acquisition window because of the presence of the impurity mentioned above; this was incorporated into the kinetic model. Data were fit using the OriginPro 7.5 software package.[56]

Time-resolved Absorption Spectroscopy. Nanosecond time-resolved absorption measurements were collected using a Nd:YAG-based laser spectrometer that has been described previously.[52] Data were acquired on thoroughly degassed CH_2Cl_2 solutions in 1 cm path length sealed quartz cuvettes. Sample absorbance was ∼0.6 at the excitation wavelength of 355 nm. Excitation energies at the sample were about 2 mJ per pulse; all data were checked for linearity with respect to pump power, and steady-state absorption spectra were acquired before and after data acquisition to ensure

(52) (a) Damrauer, N. H.; Boussie, T. R.; Devenney, M.; McCusker, J. K. *J. Am. Chem. Soc.* **1997**, *119*, 8253. (b) Juban, E. A.; McCusker, J. K. *J. Am. Chem. Soc.* **2005**, *127*, 6857.
(53) Claude, J. P.; Meyer, T. J. *J. Phys. Chem.* **1995**, *99*, 51.
(54) Parker, C. A.; Rees, W. T. *Analyst (London)* **1960**, *85*, 587.
(55) DeWitt, L.; Blanchard, G. J.; LeGoff, E.; Benz, M. E.; Liao, J. H.; Kanatzidis, M. G. *J. Am. Chem. Soc.* **1993**, *115*, 12158.
(56) *Origin*, 7.5th ed.; OriginLab Corp.: Northhampton, MA, 1991− 2004.

the integrity of the sample. Differential absorption spectra were generated by plotting the amplitudes of fits of the decay kinetics acquired as a function of probe wavelength.

Subnanosecond time-resolved data were obtained for complex **1** using a femtosecond time-resolved absorption spectrometer that is described elsewhere.[52b] Samples were dissolved in CH_2Cl_2 in an Ar atmosphere drybox and placed in 1 mm path length quartz cuvettes with absorbance values of ~0.6 at the excitation wavelength (λ_{pump} = 370 nm). Single-wavelength kinetics data were collected at λ_{probe} = 700 nm following ~100 fs excitation at 370 nm with a pump power of about 4 μJ. Single-photon excitation was confirmed by the linearity of the signal response with respect to pump power. Acquisition of full spectra for complex **1** was hampered by the formation of a photoproduct that precipitated over the course of several hours of data acquisition. Nevertheless, the data were sufficient to establish that identical kinetics are observed across the entire visible probe window; this will be elaborated upon in the Results and Discussion section. All data were fit using programs of local origin.

Förster Energy Transfer Rate Calculations. Calculations of energy transfer rates were carried out based on eqs 1–3. Donor−acceptor distances and angles were measured using the single-crystal X-ray structure data of complex **2** with the Diamond 3.1d crystal structure and visualization software.[57]

Results and Discussion

Synthesis and Characterization. Our interest in these systems was to investigate energy and/or electron transfer processes in structurally well-defined polynuclear charge-transfer assemblies. The choice of using Re^{I} and Fe^{III} was based on the well-known MLCT-based reactivity of Re^{I} and the propensity for Fe^{III} to act as both an energy and electron acceptor.[58–63] The utilization of the $M(pyacac)_3$ core (M = Fe^{III} and Al^{III}) as a ligand for $Re(bpy')(CO)_3(OTf)$ allowed the pyridyl group to displace the weakly coordinating triflate anion and generate the tricationic $FeRe_3$ and $AlRe_3$ complexes. The formation of the tetranuclear assemblies was facilitated by the low steric crowding afforded by the roughly 120° separation of the three pyacac ligands.

The ESI-MS data for complexes **1**−**6** in acetonitrile solution are consistent with the formation of the desired $FeRe_3$ and $AlRe_3$ assemblies. For example, complex **2** shows peaks corresponding to $\{[Fe(pyacac)_3(Re(bpy)(CO)_3)_3]\}^{3+}$, $\{[Fe(pyacac)_3(Re(bpy)(CO)_3)_3](OTf)\}^{2+}$, and $\{[Fe(pyacac)_3(Re(bpy)(CO)_3)_3](OTf)_2\}^{+}$. X-ray quality crystals for complexes **2** and **5** were generated by diffusion of ether into an acetonitrile solution of the complexes over the course of approximately 1 week; this in turn provides additional evidence for the general robustness of complexes **1**−**6** in solution. Nevertheless, the Fe^{III}-containing complexes **1**−**3** were found to be susceptible to slight decomposition in the presence of water. As mentioned in the Experimental Section, this was established via single-photon counting emission spectroscopy through the detection of a highly emissive, long-lived excited-state species. Because Fe^{III} compounds are nonemissive, this impurity is most likely a Re-bpy′-containing fragment resulting from displacement of the pyacac ligand by adventitious H_2O. This decomposition pathway is not too surprising given the lability of high-spin Fe^{III} and its propensity to bind H_2O, but the extremely low intensity of the TCSPC signal corresponding to this species indicates that this represents a very minor component in solution.

The ν(CO) stretching bands of the $Re(bpy')(CO)_3$ moieties (Table 3) were assigned based on previously reported data for *fac*-$[Re(4,4'\text{-}X_2\text{-}bpy)(CO)_3(4\text{-}Etpy)](PF_6)$ complexes.[64] The characteristic spectral profile consists of two very intense peaks. The broadband at lower energy corresponds to two overlapping transitions assigned to the A′(2) and A″ modes (C_s symmetry), whereas the sharper, higher energy band is assigned as A′(1).[65] The fact that the carbonyl frequencies observed for each $FeRe_3/AlRe_3$ pair are virtually identical is indicative of minimal direct electronic communication between the Re^{I} and Fe^{III} metal centers in the ground states of the $FeRe_3$ assemblies.[7]

Single-Crystal X-ray Structures. X-ray quality crystals were obtained for $[Fe(pyacac)_3(Re(bpy)(CO)_3)_3](OTf)_3$ (**2**) and $[Al(pyacac)_3(Re(bpy)(CO)_3)_3](OTf)_3$ (**5**). The two complexes are isostructural and crystallize in the triclinic space group $P\bar{1}$. Crystallographic details are given in Table 1 with selected bond distances and angles for the two complexes listed in Table 2. The coordination environments about the central metal ions in both complexes (Figure 1) are distorted octahedra with six oxygen atoms from the acac groups comprising the coordination sphere. In the case of complex **2**, the Fe−O bond distances of about 1.98 ± 0.02 Å are consistent with high-spin Fe^{III} and compare favorably with other structurally characterized examples of Fe^{III}-acac systems.[48] Significantly shorter metal−oxygen bonds (ca. 0.1 Å) are observed for complex **5**: such differences are to be expected given the smaller ionic radius of Al^{III}.[48] The structures of the $Re(bpy)(CO)_3$ moieties in both molecules are unremarkable, exhibiting the pseudo-C_{3v} coordination environment common to Re^{I} complexes in this class.[66–69] Not surprisingly, the metric details of the Re^{I} fragment are insensitive to the identity of the central metal ion: bond distances, and angles associated with the primary coordination sphere as well as within the bipyridyl ligand itself are identical within experimental error for the Fe^{III} and Al^{III} complexes. Slight differences are noted in the $Re^{I}\cdots M^{III}$ distances, with complex **5** being uniformly shorter by ~0.1

(57) Brandenburg, K.; Berndt, M. *DIAMOND*, ver 3.1d; Crystal Impact: Bonn, Germany, 2006.
(58) Lin, C. T.; Sutin, N. *J. Am. Chem. Soc.* **1975**, *97*, 3543.
(59) Lin, C. T.; Bottcher, W.; Creutz, C.; Sutin, N. *J. Am. Chem. Soc.* **1976**, *98*, 6536.
(60) Lin, C. T.; Sutin, N. *J. Phys. Chem.* **1976**, *80*, 97.
(61) Katz, N. E.; Creutz, C.; Sutin, N. *Inorg. Chem.* **1988**, *27*, 1687.
(62) Wilkinson, F.; Farmilo, A. *J. Chem. Soc., Faraday Trans.* **1976**, *72*, 604.
(63) Pettersson, K.; Kilså, K.; Mårtensson, J.; Albinsson, B. *J. Am. Chem. Soc.* **2004**, *126*, 6710.
(64) Dattelbaum, D. M.; Omberg, K. M.; Schoonover, J. R.; Martin, R. L.; Meyer, T. J. *Inorg. Chem.* **2002**, *41*, 6071.
(65) Dattelbaum, D. M.; Martin, R. L.; Schoonover, J. R.; Meyer, T. J. *J. Phys. Chem. A.* **2004**, *108*, 3518.
(66) Lucia, L. A.; Abboud, K.; Schanze, K. S. *Inorg. Chem.* **1997**, *36*, 6224.
(67) Chen, P.; Curry, M.; Meyer, T. J. *Inorg. Chem.* **1989**, *28*, 2271.
(68) Wenger, O. S.; Henling, L. M.; Day, M. W.; Winkler, J. R.; Gray, H. B. *Inorg. Chem.* **2004**, *43*, 2043.
(69) Busby, M.; Liard, D. J.; Motevalli, M.; Toms, H.; Vlček, A. *Inorg. Chim. Acta* **2004**, *357*, 167.

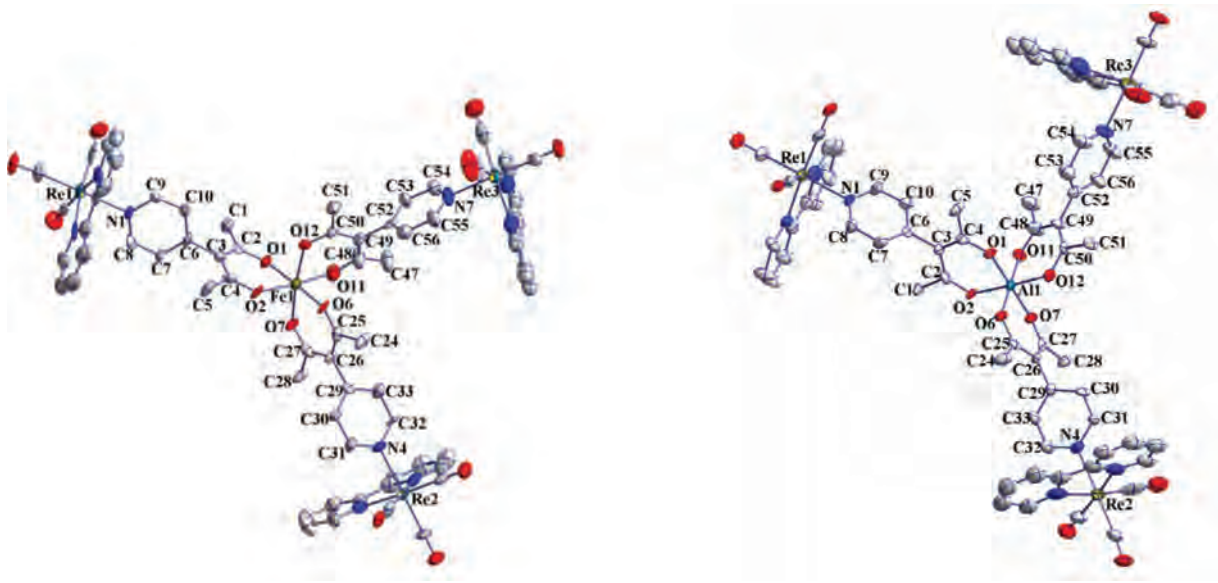

Figure 1. Drawing of the cations of $[Fe(pyacac)_3(Re(bpy)(CO)_3)_3](OTf)_3$ (**2**, left) and $[Al(pyacac)_3(Re(bpy)(CO)_3)_3](OTf)_3$ (**5**, right) obtained from single-crystal X-ray structure determinations. Atoms are represented as 50% probability thermal ellipsoids.

Å mainly because of the decrease in metal−oxygen bond lengths relative to complex **2**. Despite these minor differences, there is considerable structural homology between the two complexes, underscoring the appropriateness of using Al^{III} as a structurally and electronically benign replacement for Fe^{III} in this system. Our efforts to obtain X-ray quality crystals for complexes **1**, **3**, **4**, and **6** have thus far been unsuccessful; however, we do not expect that substituent changes on the periphery of the bipyridyl ligand will have any significant effect on the basic structural features of this system.

Electrochemistry. The electrochemical properties of complexes **1**−**6** were examined using both cyclic and differential pulse voltammetry; the data are given in Table 3. The availability of the Al^{III} model complexes greatly simplifies assigning the features observed for all six complexes because of the redox-inert nature of this ion. Accordingly, the single reduction waves seen for complexes **4**−**6** can be immediately ascribed to the bipyridyl ligand of the Re moiety in each case. The positive shift in potential across the series is consistent with the more electron withdrawing nature of the substitutients as one progresses from the methyls of tmb (**4**) to the diethylester groups in complex **6**. Similarly, the oxidation waves seen for all three complexes are easily assigned to the Re^{I}/Re^{II} couple. The influence of the bipyridyl substitutents are apparent in these data as well, with the more electron deficient ligand giving rise to the most positive oxidation potential for the Re center. The results are all consistent with what has been observed for complexes of the general form *fac*-$[Re(4,4'\text{-}X_2\text{-bpy})(CO)_3(4\text{-Etpy})](PF_6)$ previously reported in the literature.[46]

Given these assignments, the reductions at ca. −0.9 V observed for complexes **1**−**3** are clearly associated with the Fe^{III} center.[70] It can be seen that modification of the bipyridyl ligand has no discernible influence on the redox properties of the central Fe ion. In a similar vein, we note that the ligand

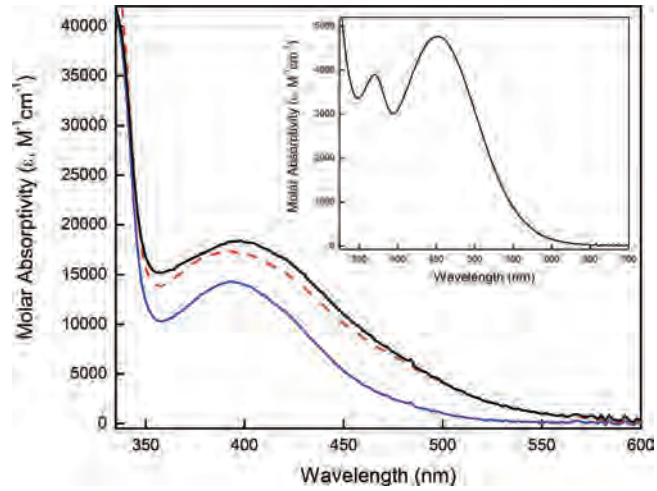

Figure 2. Electronic absorption spectra of $[Fe(pyacac)_3(Re(deeb)(CO)_3)_3](OTf)_3$ (**3**) (black trace) and $[Al(pyacac)_3(Re(deeb)(CO)_3)_3](OTf)_3$ (**6**) (blue trace) acquired in CH_2Cl_2 solution at 298 K. The dashed red trace corresponds to linear combination of the molar absorptivity profiles of the Al^{III} complex with that of $Fe(phacac)_3$ (inset).

reduction and Re^{I} oxidation potentials of all three Fe-containing compounds are essentially identical to what was observed for the Al^{II} analogs. These data are indicative of (relatively) weak electronic coupling between the central metal ion and the peripheral chromophores.

Electronic Absorption Spectroscopy. The electronic absorption spectra of complexes **1**−**6** have been acquired in room-temperature CH_2Cl_2 solutions. Spectra for complexes **3** and **6** are shown in Figure 2; all six spectral profiles can be found in Supporting Information, Figure S1. Re^{I} polypyridyl complexes are typically characterized by a $^1A_1 \rightarrow {}^1$MLCT absorption that falls in the range of approximately 330 to 430 nm[71,72] with the energy of the transition generally

(70) McCarthy, H. J.; Tocher, D. A. *Polyhedron* **1987**, *6*, 1421.

(71) Sacksteder, L.; Zipp, A. P.; Brown, E. A.; Streich, J.; Demas, J. N.; DeGraff, B. A. *Inorg. Chem.* **1990**, *29*, 4335.

(72) Worl, L. A.; Duesing, R.; Chen, P.; Della Ciana, L.; Meyer, T. J. *J. Chem. Soc., Dalton Trans.* **1991**, 849.

Table 4. Photophysical Data of Complexes **1**−**6**

compound	λ (nm)	E_{00} (cm^{-1})[a]	Φ_r	k_{obs} (s^{-1})	k_r ($\times 10^5$ s^{-1})[d]	k_{nr} ($\times 10^6$ s^{-1})[e]
$[Fe(pyacac)_3(Re(tmb)(CO)_3)_3](OTf)_3$ (**1**)	*b*	*b*	*c*	$2.3 \pm 0.1 \times 10^9$	2.3 ± 0.1[f]	0.22 ± 0.01[f]
$[Fe(pyacac)_3(Re(bpy)(CO)_3)_3](OTf)_3$ (**2**)	*b*	*b*	*c*	$1.3 \pm 0.1 \times 10^9$	2.9 ± 0.1[f]	1.5 ± 0.1[f]
$[Fe(pyacac)_3(Re(deeb)(CO)_3)_3](OTf)_3$ (**3**)	*b*	*b*	*c*	$4.0 \pm 0.1 \times 10^8$	3.0 ± 0.1[f]	4.0 ± 0.2[f]
$[Al(pyacac)_3(Re(tmb)(CO)_3)_3](OTf)_3$ (**4**)	526	19 900	0.51	$4.4 \pm 0.2 \times 10^5$	2.3 ± 0.1	0.22 ± 0.01
$[Al(pyacac)_3(Re(bpy)(CO)_3)_3](OTf)_3$ (**5**)	566	18 700	0.16	$1.8 \pm 0.1 \times 10^6$	2.9 ± 0.1	1.5 ± 0.1
$[Al(pyacac)_3(Re(deeb)(CO)_3)_3](OTf)_3$ (**6**)	624	16 800	0.07	$4.3 \pm 0.2 \times 10^6$	3.0 ± 0.1	4.0 ± 0.2

[a] Zero-point energy difference between ^{3}MLCT excited state and ground state based on spectral fitting analysis. [b] This value is expected to be identical to the corresponding Al^{III} complex. [c] Values are not quoted because of the presence of an emissive impurity. See text for further details. [d] $k_r = k_{obs} * \Phi_r$. [e] $k_{nr} = k_{obs} - k_r$. [f] k_r and k_{nr} values are anticipated to be similar to the corresponding Al^{III} complex.

reflecting the electron donating/withdrawing ability of the bpy substituents. The $^1A_1 \rightarrow {}^1$MLCT absorption of the $Re(deeb)(CO)_3$ chromophore is evident in Figure 2 with $\lambda_{max} = 394$ nm; as the substituents become progressively more electron donating (e.g., H for bpy and CH_3 for tmb) this feature systematically shifts to the blue and begins to overlap with the ligand-based absorptions in the ultraviolet (Supporting Information, Figure S1).

The presence of Fe^{III} in complexes **1**−**3** gives rise to a new, broad absorption feature on the low-energy side of the Re^I-based charge-transfer band. The inset of Figure 2 shows the absorption spectrum of $Fe(phacac)_3$ which exhibits two strong transitions centered at 370 and 460 nm assigned as $^6A_1 \rightarrow {}^6$MLCT and $^6A_1 \rightarrow {}^6$LMCT transitions, respectively.[73,74] In complexes **1**−**3** the higher energy MLCT absorption is obscured by the more intense $^1A_1 \rightarrow {}^1$MLCT band of the Re^I chromophore, but the low energy tail of the $^6A_1 \rightarrow {}^6$LMCT transition can be seen extending out to approximately 600 nm. A linear combination of the spectrum of the Al^{III} analogue with that of $Fe(phacac)_3$ (dashed red line) confirms that the ground-state absorption spectra of these complexes can be viewed in terms of a superposition of contributions from the Re^I and Fe^{III} fragments.

Steady-State and Time-Resolved Emission. The $AlRe_3$ complexes represent an ideal model for dynamics that may occur in the corresponding $FeRe_3$ systems because of their similar structural features and the inability of Al^{III} to engage in excited-state processes such as electron or energy transfer. Emission spectra for complexes **4**−**6** were acquired at room temperature in deoxygenated CH_2Cl_2 and are plotted in Supporting Information, Figure S2. The spectral profiles correspond well to previously reported photophysical studies of Re^I polypyridyl systems, with the emission assigned as a ^{3}MLCT $\rightarrow {}^1A_1$ transition.[75] The change in energy gap across the series due to differences in the electron donating/withdrawing ability of the substituents is reflected in the radiative quantum yields, dropping by a factor of ~7 from complex **4** ($\Phi_r = 0.51$) to complex **6** ($\Phi_r = 0.07$); these values are comparable to those reported for the corresponding mononuclear Re^I polypyridyl derivatives.[46] Time-resolved emission data for complexes **4**−**6** could all be fit to single-exponential decay models. The kinetics reveal that the reduction in quantum yield is due primarily to an increase in the nonradiative decay rate for ^{3}MLCT relaxation (k_{nr}) as opposed to significant variations in radiative coupling to the ground state (Table 4). As with the quantum yields, the observed excited-state lifetimes and rate constants are all consistent with the assignment of ^{3}MLCT $\rightarrow {}^1A_1$ emission reported previously for the mononuclear Re^I polypyridyl derivatives.[46,76]

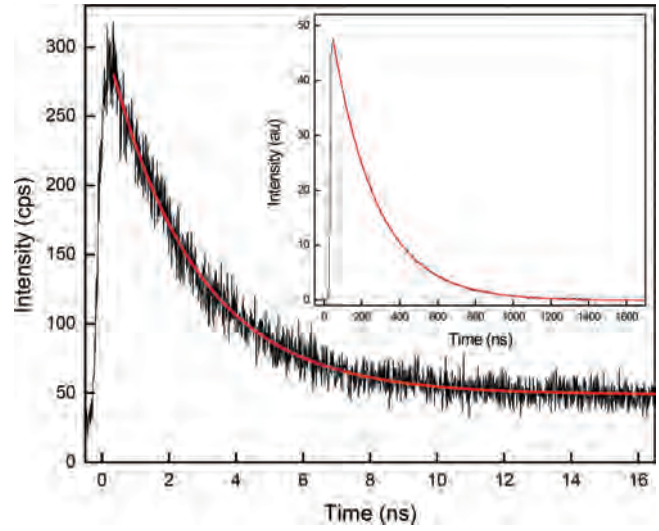

Figure 3. TCSPC emission data for $[Fe(pyacac)_3(Re(deeb)(CO)_3)_3](OTf)_3$ (**3**) acquired in CH_2Cl_2 solution at 298 K. The emission was monitored at $\lambda_{probe} = 624$ nm following excitation at $\lambda_{pump} = 430$ nm. The solid red line corresponds to a fit to a single-exponential decay model with $\tau_{obs} = 2.5 \pm 0.1$ ns. The inset shows nanosecond time-resolved emission data for the corresponding model complex, $[Al(pyacac)_3(Re(deeb)(CO)_3)_3](OTf)_3$ (**6**), with $\tau_{obs} = 235 \pm 20$ ns.

Steady-state emission spectra were also acquired for complexes **1**−**3**. Although the data indicated significantly weaker emission from each of the $FeRe_3$ complexes as compared to their $AlRe_3$ analogues, suggesting efficient quenching by the Fe^{III} core, the measured quantum yields were not reproducible. As mentioned in the Experimental Section, we believe this is due to the presence of a small amount of dissociated complex in solution caused by displacement of the pyacac ligand from the Fe^{III} core.

The lack of a readily identifiable steady-state signal from the intact $FeRe_3$ assemblies prompted the use of time-resolved methods to quantify the degree of excited-state quenching in complexes **1**−**3**. A plot of the data obtained for complex **3** is shown in Figure 3; data for all three Fe^{III}-containing compounds are plotted in Supporting Information, Figure S3. The signal-to-noise ratio is relatively poor owing to a combination of virtually complete quenching of the Re^I-based ^{3}MLCT states coupled with radiative rate constants

(73) Lintvedt, R. L.; Kernitsky, L. K. *Inorg. Chem.* **1970**, *9*, 491.
(74) Barnum, D. W. *J. Inorg. Nucl. Chem.* **1961**, *21*, 221.
(75) Striplin, D. R.; Crosby, G. A. *Chem. Phys. Lett.* **1994**, *221*, 426.
(76) Kestell, J. D.; Williams, Z. L.; Stultz, L. K.; Claude, J. P. *J. Phys. Chem. A.* **2002**, *106*, 5768.

that are on the order of 10^5 s^{-1}. Nevertheless, emission decays for each of the $FeRe_3$ complexes could be fit to single-exponential kinetics with $\tau_{obs} = 450 \pm 30$ ps, 755 ± 40 ps, and 2.5 ± 0.1 ns for complexes **1**, **2**, and **3**, respectively (Table 4). These time constants are several orders of magnitude shorter than what was observed for the Al^{III} model complexes, indicating that excited-state relaxation in complexes **1**−**3** is dominated by reaction with the Fe^{III} core. The rate constant for the reaction is given by eq 5,

$$k_q^{FeRe_3} = k_{obs}^{FeRe_3} - k_{obs}^{AlRe_3} \quad (5)$$

where the values of k_r and k_{nr} for the ^{3}MLCT excited state of a given $FeRe_3$ assembly are taken to be equivalent to the corresponding $AlRe_3$ model complex. Given the extensive quenching of the ^{3}MLCT state as indicated by the time constant for decay in complexes **1**-**3**, the observed lifetimes effectively correspond to the quenching time constants in all three cases.

Mechanistic Considerations: Electron versus Energy Transfer Quenching. Both electron and energy transfer processes can be envisioned to occur out of the Re^I-based ^{3}MLCT excited state. On the basis of the presence of Fe^{III} in the ground states of these complexes, electron transfer would proceed as an oxidative quenching reaction to produce a Re^{II}/Fe^{II} charge separated species. $Re^I \rightarrow Re^{II}$ oxidation and $Fe^{III} \rightarrow Fe^{II}$ reduction potentials for complexes **1**−**3** (Table 3), along with the zero-point energy gaps of the ^{3}MLCT states (E_{00}) determined from fits of the emission spectra of the corresponding $AlRe_3$ analogues (Table 4), were used to determine the thermodynamic driving force for photoinduced electron transfer.[77,78] These calculations revealed that electron transfer is unfavorable for complexes **2** and **3** (~0 and +0.45 eV, respectively) and only slightly exothermic in the case of complex **1** (−0.1 eV). The magnitude of ΔG^{ET} for complex **3** is prohibitively large, particularly given the observed rate constant of nearly 10^9 s^{-1}. In the case of complex **2**, electron transfer is thermodynamically feasible; however, the fact that the quenching rate is only a factor of ~3 faster than what is observed for complex **3** suggests that both of these complexes are reacting via similar mechanisms, namely, energy transfer.

The fact that electron transfer is predicted to be exothermic in the case of complex **1** prompted further study. We therefore carried out time-resolved absorption measurements on $[Fe(pyacac)_3(Re(tmb)(CO)_3)_3](OTf)_3$ (**1**) in an effort to identify whether a charge-separated species was being formed upon $^1A_1 \rightarrow {}^1$MLCT excitation. The transient absorption spectroscopy of Re^I polypyridyl complexes has been described by a number of workers.[79–86] Their excited-state spectra typically consist of a moderately intense feature in the ultraviolet corresponding to absorptions of the polypyridyl radical anion, as well as a transient bleach due to loss of the ground-state $^1A_1 \rightarrow {}^1$MLCT absorption. Additional absorptions can also be observed toward the red edge of the visible spectrum that are usually ascribed to bpy^- transitions of the excited-state species. Consistent with these expectations, the differential absorption spectrum of $[Al(pyacac)_3(Re(tmb)(CO)_3)_3](OTf)_3$ (**4**) (Figure 4, top) exhibits transient absorptions at 370 and 760 nm that we assign to tmb^--based transitions. The hallmark for an excited-state electron transfer process in complex **1** would be a wavelength-dependence in the observed kinetics, namely, the loss of the tmb^- features coupled with a persistence of the ground-state $^1A_1 \rightarrow {}^1$MLCT

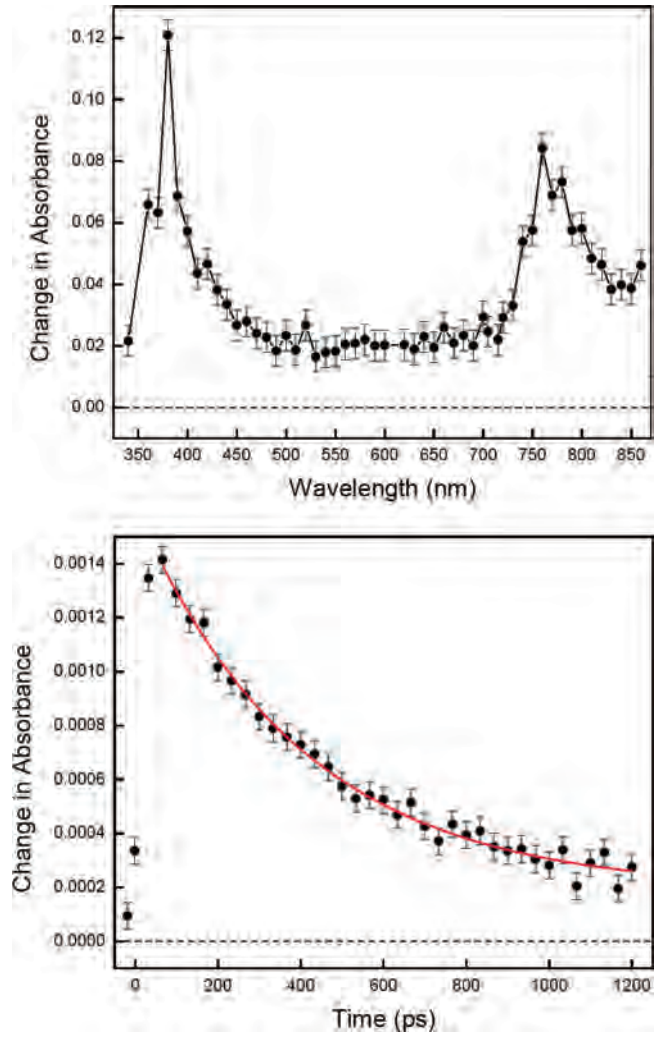

Figure 4. Top: nanosecond time-resolved differential absorption spectrum of $[Al(pyacac)_3(Re(tmb)(CO)_3)_3](OTf)_3$ (**4**) in room temperature CH_2Cl_2 solution. The spectrum was constructed from the amplitudes of fits to single-exponential decay kinetics at each probe wavelength following excitation at 355 nm. Bottom: time-resolved absorption data for $[Fe(pyacac)_3(Re(tmb)(CO)_3)_3](OTf)_3$ (**1**) in room-temperature CH_2Cl_2 solution at $\lambda_{probe} = 700$ nm following ~100 fs excitation at $\lambda_{pump} = 400$ nm. The red solid line corresponds to a fit of the data to a single-exponential decay model with $\tau_{obs} = 400 \pm 30$ ps.

(77) Rehm, D.; Weller, A. *Isr. J. Chem.* **1970**, *8*, 259.
(78) The Rehm−Weller equation for this system is given as $\Delta G^{ET} = E_{ox}(Re^{I/II}) - E_{red}(Fe^{III/II}) - E_{00}$, where E_{00} is the energy gap between the ground and lowest energy ^{3}MLCT excited state of the donor.
(79) Chen, P.; Westmoreland, T. D.; Danielson, E.; Schanze, K. S.; Anthon, D.; Neveux, P. E.; Meyer, T. J. *Inorg. Chem.* **1987**, *26*, 1116.
(80) Lin, R.; Guarr, T. F.; Duesing, R. *Inorg. Chem.* **1990**, *29*, 4169.
(81) Tapolsky, G.; Duesing, R.; Meyer, T. J. *Inorg. Chem.* **1990**, *29*, 2285.
(82) Tapolsky, G.; Duesing, R.; Meyer, T. J. *J. Phys. Chem.* **1991**, *95*, 1105.
(83) Abbott, L. C.; Arnold, C. J.; Ye, T.; Gordon, K. C.; Perutz, R. N.; Hester, R. E.; Moore, J. N. *J. Phys. Chem. A* **1998**, *102*, 1252.
(84) Liard, D. J.; Vlček, A. *Inorg. Chem.* **2000**, *39*, 485.
(85) Liard, D. J.; Busby, M.; Matousek, P.; Towrie, M.; Vlček, A. *J. Phys. Chem. A* **2004**, *108*, 2363.
(86) Busby, M.; Gabrielsson, A.; Matousek, P.; Towrie, M.; Di Bilio, A. J.; Gray, H. B.; Vlček, A. *Inorg. Chem.* **2004**, *43*, 4994.

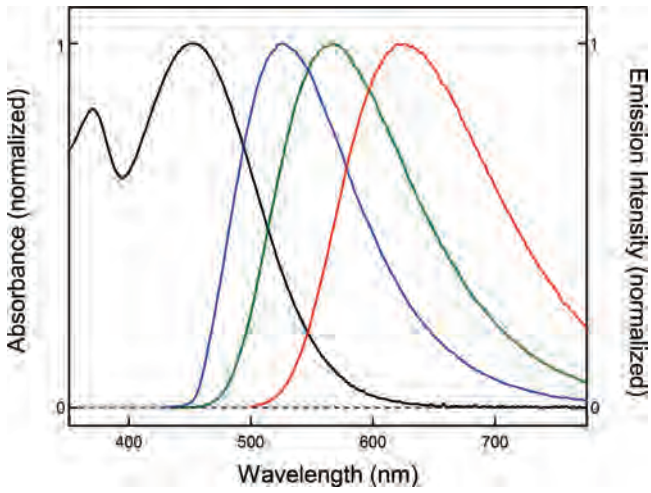

Figure 5. Overlay of the emission spectra of $[Al(pyacac)_3(Re(tmb)(CO)_3)_3](OTf)_3$ (**4**, blue), $[Al(pyacac)_3(Re(bpy)(CO)_3)_3](OTf)_3$ (**5**, green), and $[Al(pyacac)_3(Re(deeb)(CO)_3)_3](OTf)_3$ (**6**, red) with the electronic absorption spectrum of $Fe(phacac)_3$ (black). Data were acquired in CH_2Cl_2 solution at 298 K. See text for further details.

bleach. Instead, what we observe is complete ground-state recovery at all probe wavelengths with a time constant that is within experimental error of what was measured via time-resolved emission spectroscopy (Figure 4, bottom). We have recently discussed the notion that this observation does not necessarily rule out a sequential electron transfer process.[87] In the present case, however, the driving force for charge-recombination would place the back-reaction deep enough into the inverted region such that the relative rates necessary to satisfy this condition are not likely to be realized.

In light of these observations, the most likely explanation for ^{3}MLCT quenching in all three of the $FeRe_3$ assemblies is excited-state energy transfer. As discussed in the Introduction, the Dexter mechanism requires orbital overlap between the donor and acceptor involved in the energy transfer. The X-ray structure data for complex **2** shows a $Re^{I}\cdots Fe^{III}$ separation of nearly 10 Å, a value that lies at the limit of what is typically considered for an exchange-based process.[87–90] The lack of significant electronic coupling between the Re^{I} and Fe^{III} subunits is also supported by the similarities in ν(CO) frequencies of the $FeRe_3$ and $AlRe_3$ analogues, as well as the fact that the absorption spectra of the $FeRe_3$ assemblies can be represented in terms of a simple linear combination of its constituents (Figure 2). The applicability of the Förster mechanism is supported by the moderate degree of spectral overlap that exists between the Re^{I}-based ^{3}MLCT emission and the Fe^{III}-based $^6A_1 \rightarrow {}^6$LMCT absorption:[91] this is depicted graphically in Figure 5. We note that the qualitative changes in spectral overlap parallel the trend in rate constants for energy transfer determined from time-resolved emission measurements (Figure 4), which strongly implicates Förster transfer as the dominant quenching mechanism in this system.

(87) Soler, M.; McCusker, J. K. *J. Am. Chem. Soc.* **2008**, *130*, 4708.
(88) Wang, Y.; Schanze, K. S. *Inorg. Chem.* **1994**, *33*, 1354.
(89) Bignozzi, C. A.; Bortolini, O.; Chiorboli, C.; Indelli, M. T.; Rampi, M. A.; Scandola, F. *Inorg. Chem.* **1992**, *31*, 172.
(90) Berg, K. E.; Tran, A.; Raymond, M. K.; Abrahamsson, M.; Wolny, J.; Redon, S.; Andersson, M.; Sun, L.; Styring, S.; Hammarström, L.; Toftlund, H.; Åkermark, B. *Eur. J. Inorg. Chem.* **2001**, 1019.

Quantifying Förster Transfer. The spectral properties of the $FeRe_3$ family of complexes combined with the structural rigidity of the system provides a rare opportunity to quantitatively apply Förster theory and compare calculated rates with those obtained experimentally. In addition to the overlap factor alluded to above, the rate of energy transfer is also sensitive to the relative orientation of the donor and acceptor transition dipoles (eq 3). An accurate determination of this quantity can be quite challenging. In one noteworthy example, Fleming and co-workers utilized time-dependent density functional theory (TD-DFT) to enable them to visualize the transition dipoles of peridinin, which in turn provided them with tremendous insights into the role geometry plays in facilitating energy transfer from the singlet excited state(s) of that system.[92] Unfortunately, the complicated electronic structures of transition-metal containing systems do not easily lend themselves to a similarly detailed analysis, so more approximate methods must usually be employed.

An excellent example of this is that of Harriman and co-workers, in which Förster energy transfer dynamics in Ru^{II} and Os^{II} polypyridine donor−acceptor complexes bridged by a rigid spiro-based spacer moiety were investigated.[93] In their approach, energy-minimized structures were calculated for each molecule with the donor and acceptor transition dipole moments modeled along the six respective Ru−N and Os−N bond vectors. Using this geometric picture, calculations of donor−acceptor separations (R_{DA}) and orientation factors (κ^2) afforded a theoretical Förster rate constant that agreed very closely with the experimentally observed values. We have taken a similar approach for analyzing the $FeRe_3$ family of complexes, albeit with slight differences in the physical description of the system. For example, we have chosen to approximate the donor and acceptor transition dipoles as bisecting the local C_2 axes of the bpy′ and acac

Chart 1

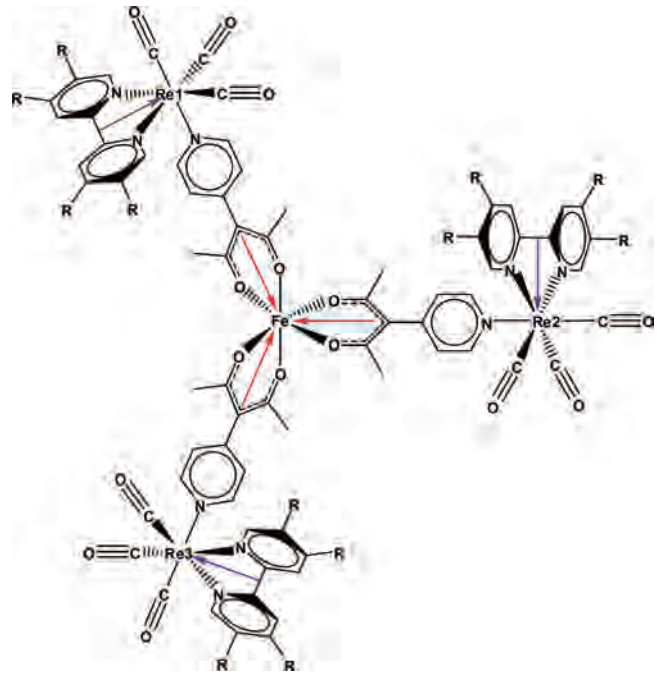

Chart 2

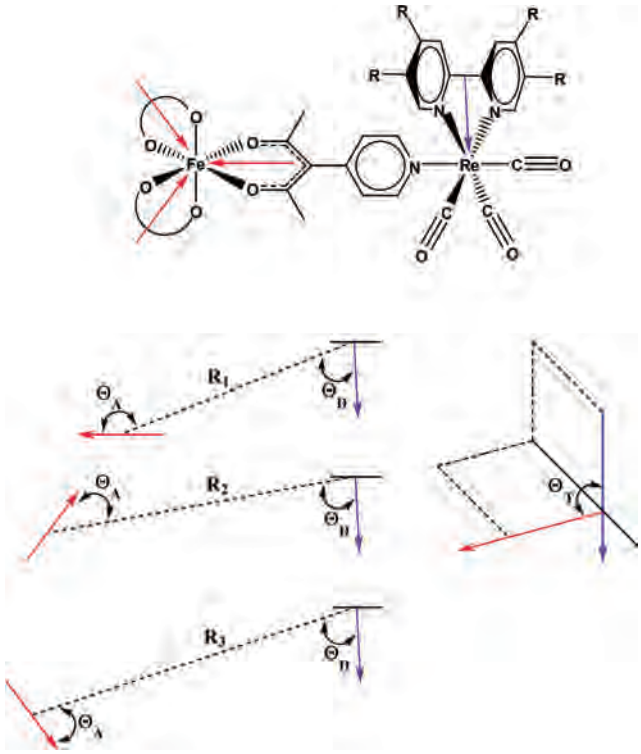

Chart 3

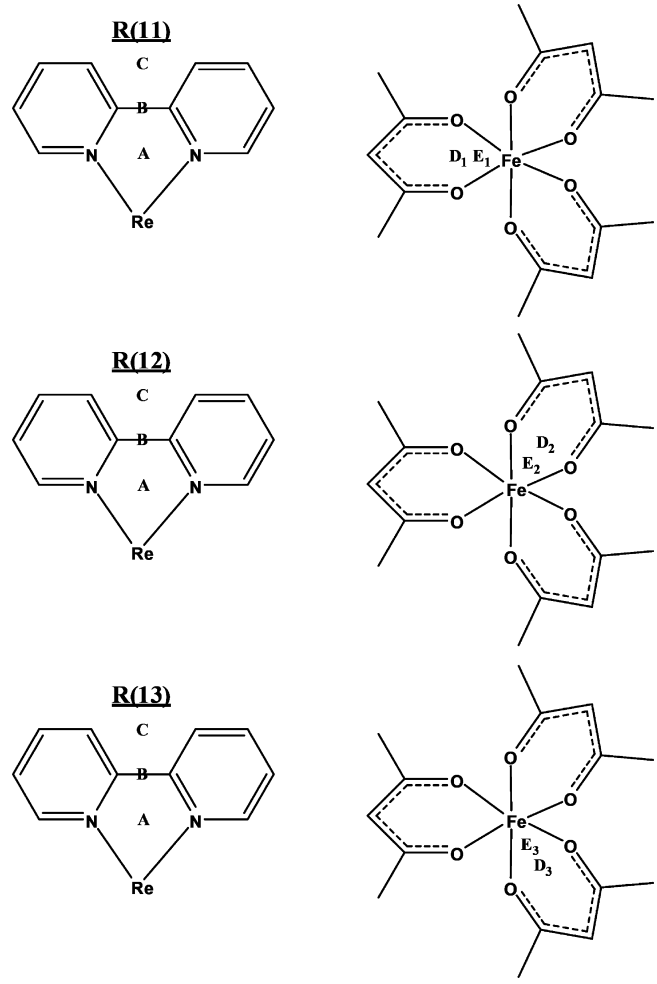

ligands as opposed to them lying coincident with the metal−ligand bond vectors. In addition, the point of origin for the transition moment dipoles has been modeled to originate solely from the ligands involved in the donor and acceptor transitions. These choices are based largely on DFT calculations on $[Ru(bpy)_3]^{2+}$ by Daul et al.[94] and Gorelsky and Lever[95] that suggest the lowest energy excited state (^{3}MLCT) is localized on the bpy ligands. In addition, Meyer and co-workers have shown that the majority of the amplitude of the thermalized ^{3}MLCT wave function for complexes of the form *fac*-[Re(4,4′-X_2-bpy)$(CO)_3$(4-Et-py)](PF_6) (X = CH_3, H, and CO_2Et) is concentrated within the π^* levels of the bpy′ ligand and less so along the Re−N bond vector.[65]

Our model is illustrated in Charts 1–3. The emission dipoles of all three Re^I donors (i.e., Re1, Re2, and Re3) are presented simultaneously for clarity in Chart 1, but only a single Re^I moiety is considered to be involved in a given excited-state quenching event because of the low excitation photon flux used for the steady-state and time-resolved emission measurements (Chart 2). The presence of three $^6A_1 \rightarrow {}^6$LMCT absorption dipoles in the Fe^{III} core gives rise to a set of vectors (R_1, R_2, and R_3) and angles (Θ_T, Θ_D, and Θ_A) for each Re^I fluorophore. The charge-transfer nature of the donor and acceptor transitions makes it difficult to place an exact point of origin for each, so distance and orientation factors were calculated for a range of possible loci for both the donor and acceptor (Chart 3). Thus, the individual Förster rate constants for a given fluorphore (Re1, Re2, or Re3) were determined for a particular origin associated with the donor (e.g., A, B, or C) interacting with a specific acceptor point associated with the $Fe(pyacac)_3$ core (D, E, and F, the Fe center). This approach yielded a total of 81 donor−acceptor interactions (27 for each Re^I fluorophore), each being defined by specific R_{DA} and κ^2 values that were evaluated based on the single-crystal X-ray structure data of complex **2**. A complete list of the values of R_{DA} and κ^2 used in our analysis can be found in the Supporting Information.

The analysis we have carried out is predicated on two critical assumptions: (1) that the variations in substitutents on the peripheral bipyridine group do not significantly alter the metrics relevant for dipolar energy transfer (thereby allowing us to use the X-ray structure of complex **2** as the basis for analyzing all three $FeRe_3$ assemblies), and (2) that the geometry of each compound in solution is essentially unchanged from that determined by solid-state X-ray crystallography. The major influence of the bipyridyl substituents will be to shift the electron density associated with the excited state according to the electron donating/withdrawing ability of the group. This assertion is supported by structure

(91) Yardley, J. T. *Introduction to Molecular Energy Transfer.*; Academic Press: New York, 1980.
(92) Vaswani, H. M.; Hsu, C.-P.; Head-Gordon, M.; Fleming, G. R. *J. Phys. Chem. B.* **2003**, *107*, 7940.
(93) Juris, A.; Prodi, L.; Harriman, A.; Ziessel, R.; Hissler, M.; El-ghayoury, A.; Wu, F.; Riesgo, E. C.; Thummel, R. P. *Inorg. Chem.* **2000**, *39*, 3590.
(94) Daul, C.; Baerends, E. J.; Vernooijs, P. *Inorg. Chem.* **1994**, *33*, 3538.
(95) Gorelsky, S. I.; Lever, A. B. P. *J. Organomet. Chem.* **2001**, *635*, 187.

Table 5. Calculated Förster Rate Constants for $[Fe(pyacac)_3(Re(tmb)(CO)_3)_3](OTf)_3$ (**1**), $[Fe(pyacac)_3(Re(bpy)(CO)_3)_3](OTf)_3$ (**2**), and $[Fe(pyacac)_3(Re(deeb)(CO)_3)_3](OTf)_3$ (**3**)

	interaction[a]	complex **1**[b] k_T (s^{-1})	complex **2**[b] k_T (s^{-1})	complex **3**[b] k_T (s^{-1})
	Re1:LMCT1	3.6×10^8	3.3×10^8	5.5×10^7
	Re1:LMCT2	2.9×10^8	2.7×10^8	4.4×10^7
	Re1:LMCT3	1.3×10^8	1.2×10^8	1.9×10^7
k_{Re1} (s^{-1})[c]		7.8×10^8	7.2×10^8	1.2×10^8
	Re2:LMCT1	3.1×10^8	2.8×10^8	4.7×10^7
	Re2:LMCT2	3.1×10^8	2.8×10^8	4.6×10^7
	Re2:LMCT3	1.4×10^8	1.3×10^8	2.2×10^7
k_{Re2} (s^{-1})[c]		7.6×10^8	6.9×10^8	1.2×10^8
	Re3:LMCT1	1.2×10^8	1.3×10^8	1.8×10^7
	Re3:LMCT2	3.9×10^8	3.6×10^8	5.9×10^7
	Re3:LMCT3	5.3×10^8	4.9×10^8	8.0×10^7
k_{Re3} (s^{-1})[c]		1.0×10^9	9.8×10^8	1.6×10^8
$\langle k_T \rangle$ (s^{-1})[d]		8.5×10^8	8.0×10^8	1.3×10^8
k_{obs} (s^{-1})		2.3×10^9	1.3×10^9	4.0×10^8

[a] Donor−acceptor through-space interaction as defined in the text and in Chart 3. [b] R_{DA} and κ^2 values derived from the single-crystal X-ray data for complex **2** using the geometries outlined in Charts 1 and 2. A complete list of calculated rate constants for complexes **1**−**3** can be found in Supporting Information, Tables S4−S6. [c] Rate of energy transfer calculated according to eqs 6a–6c. [d] The overall rate of energy transfer given by ($k_{Re1} + k_{Re2} + k_{Re3}$)/3.

minimizations which revealed virtually identical bond distances and angles for all three complexes.[96] Given the distribution of anchoring points on the bipyridyl ring that we are evaluating, we believe this first issue is being adequately addressed. In terms of solution versus solid-state geometry, the only significant degree of freedom in these systems is rotation along the Re−N (pyridine) bond. We expect there will be some barrier to this motion, but it is unlikely to afford the same average angle in solution as found in the solid state. Even though this represents a possible difference in the structure of the compound between what we measure in the solid-state versus what exists in solution, an analysis of this motion revealed that the relative distances and orientations of the donor and acceptor transition dipoles (and therefore R_{DA} and κ^2) do not change over the entire 360° that the system can sample. Therefore, while in principle using a solid-state structure to model geometric properties in solution can be problematic, the particular structural aspects of the $FeRe_3$ family of complexes makes such a comparison very straightforward.

A given Re^I donor can couple to any of the three Fe^{III}-pyacac acceptor dipoles: the energy transfer process in these compounds can thus be described in terms of three parallel reactions. The overall rate constant for such a kinetic model is given by a linear combination of the rate constants for each reaction pathway as shown in eqs 6a–6c,

$$k_{Re(11)} + k_{Re(12)} + k_{Re(13)} = k_{Re1} \quad (6a)$$

$$k_{Re(21)} + k_{Re(22)} + k_{Re(23)} = k_{Re2} \quad (6b)$$

$$k_{Re(31)} + k_{Re(32)} + k_{Re(33)} = k_{Re3} \quad (6c)$$

where $k_{Re(ij)}$ corresponds to the rate calculated for the ith Re donor coupling to the jth Fe-pyacac acceptor; each of the $k_{Re(ij)}$ values derives from the average of the nine possible donor−acceptor vectors defined by the point-dipole origins depicted in Chart 3. Table 5 lists all nine $k_{Re(ij)}$ values for complexes **1**−**3** along with their average, $\langle k_T \rangle$, which we take to be the overall theoretical rate constant from our model. It can be seen that there are variations in the calculated rates of energy transfer within each group of interactions owing to slight geometric differences at each Re-bpy site. Nevertheless, despite the lack of a quantitative picture of wave functions for the donor and acceptor charge-transfer states, we consider the level of agreement we have obtained between experiment and theory—less than a factor of 3 across the entire series—to be quite good and further supports our assignment of Förster transfer.

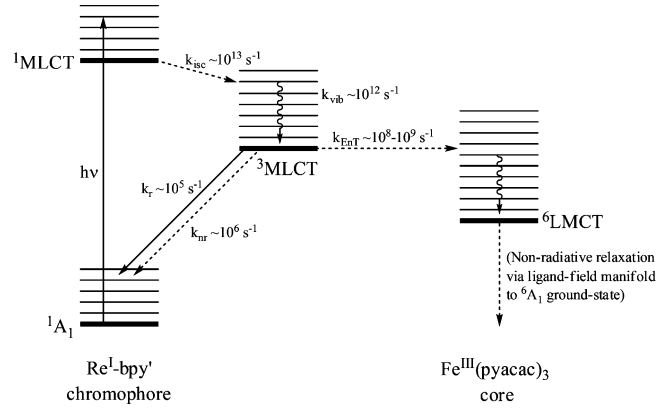

Figure 6. Energy level diagram depicting the excited-state dynamics of the $FeRe_3$ assemblies described in this paper. The rate constants for ^{1}MLCT → ^{3}MLCT intersystem crossing and vibrational cooling within the ^{3}MLCT state are based on the work of Vlček and co-workers (cf. 85), whereas the other time constants represent approximate values for complexes **1**−**6**.

The results of this study allow us to construct a comprehensive picture of the excited-state energies and dynamics for these $FeRe_3$ systems (Figure 6). The left side of Figure 6 is an energy level diagram for the relevant electronic states of the Re^I-bpy′ chromophore, along with kinetic pathways associated with the various excited states. Initial population of the ^{1}MLCT excited state is followed by rapid intersystem crossing (k_{isc}) to the ^{3}MLCT excited state.[97,98] The thermalized triplet state can then undergo radiative (k_r) and nonradiative (k_{nr}) transitions to the $^1A_1$ ground-state, or can be quenched by the Fe^{III} core via Förster energy transfer (k_{EnT}). The right side of Figure 6 shows the electronic structure of the $Fe(pyacac)_3$ core, which contains charge-transfer (^{6}LMCT) and ligand-field electronic excited states that are thermodynamically accessible from the ^{3}MLCT manifold of the Re chromophore. Dipolar energy transfer results in the formation of a ^{6}LMCT excited state within the $Fe(pyacac)_3$ core, followed by nonradiative relaxation to the $^6A_1$ ground-state of the Fe^{III} moiety.

Conclusions

The synthesis, structures, and photophysical properties of a series of donor−acceptor complexes based on Re^I-bpyridine

(96) *Spartan '02*; Wavefunction Inc.: Irvine, CA, 1991−2001.

(97) Busby, M.; Matousek, P.; Towrie, M.; Vlček, A. *J. Phys. Chem. A.* **2005**, *109*, 3000.

(98) Damrauer, N. H.; Cerullo, G.; Yeh, A.; Boussie, T. R.; Shank, C. V.; McCusker, J. K. *Science* **1997**, *275*, 54.

donors and Fe^{III}-acac acceptors have been described. Steady-state and time-resolved emission spectroscopies indicated that the strongly emissive Re^{I}-based ^{3}MLCT excited state was significantly quenched when compared to model complexes in which the Fe^{III} center had been replaced by Al^{III}. The favorable overlap between the donor emission and acceptor absorption profiles coupled with a ~10 Å donor−acceptor separation, unfavorable driving forces for electron transfer, and the absence of features characteristic of charge separation in the transient absorption spectra allowed for an assignment of Förster (dipolar) energy transfer as the dominant excited-state reaction mechanism. The well-defined structural aspects of this system permitted a quantitative geometric analysis of the dipole−dipole coupling giving rise to the observed dynamics. The calculated energy transfer rate constants differed from the experimental values by less than a factor of 3, a level of agreement that is significantly better than what is typically encountered. In addition to providing quantitative support for Förster transfer in this system, this study also demonstrates the degree of accuracy that can be achieved if the metric details concerning dipole−dipole interactions can be explicitly described.

Acknowledgment. The authors wish to thank Professor Gary Blanchard for use of the time-correlated single photon counting spectrometer and for insightful discussions, as well as Allison Brown for help in the acquisition of the femtosecond time-resolved absorption data. This work was supported with funds from the National Science Foundation under Grant CHE-0616340.

Supporting Information Available: Electronic absorption spectra for complexes **1**−**6** (Figure S1), steady-state emission spectra for complexes **1**−**6** (Figure S2), and time-resolved emission spectra for complexes **1**−**6** (Figure S3). R_{DA}, Θ_T, Θ_D, Θ_A, and κ^2 values calculated from the X-ray structural data of complex **2** for all A:D, B:D, and C:D interactions (Table S1), for all A:E, B:E, and C:E interactions (Table S2), and for all A:F, B:F, and C:F interactions (Table S3), as well as the corresponding calculated Förster rate constants (Tables S4−S6). Crystallographic data for complexes **2** and **5** in cif format are also available. This material is available free of charge via the Internet at http://pubs.acs.org.

IC800670B